SECURITY CLASSIFICATION OF THIS PAGE

REPORT DOCUMENTATION PAGE

AD-A219 786

Unclassified

1b. RESTRICTIVE MARKINGS: N/A	
2a. SECURITY CLASSIFICATION AUTHORITY: N/A	3. DISTRIBUTION/AVAILABILITY OF REPORT: Distribution Unlimited
2b. DECLASSIFICATION/DOWNGRADING SCHEDULE: N/A	
4. PERFORMING ORGANIZATION REPORT NUMBER(S): N/A	5. MONITORING ORGANIZATION REPORT NUMBER(S): AFOSR-TR- 90-0337
6a. NAME OF PERFORMING ORGANIZATION: Oklahoma State University; 6b. OFFICE SYMBOL (If applicable):	7a. NAME OF MONITORING ORGANIZATION: Air Force Office of Scientific Research
6c. ADDRESS (City, State, and ZIP Code): Department of Physics, Stillwater, OK 74078	7b. ADDRESS (City, State, and ZIP Code): Building 410, Bolling AFB, DC 20332-6448
8a. NAME OF FUNDING/SPONSORING ORGANIZATION: AFOSR; 8b. OFFICE SYMBOL (If applicable):	9. PROCUREMENT INSTRUMENT IDENTIFICATION NUMBER: AFOSR-85-0270
8c. ADDRESS (City, State, and ZIP Code): Building 410, Bolling AFB, DC 20332-6448	10. SOURCE OF FUNDING NUMBERS: PROGRAM ELEMENT NO. 61102F; PROJECT NO. 2305; TASK NO. B1; WORK UNIT ACCESSION NO.

11. TITLE (Include Security Classification)

Photorefractive Damage Mechanisms in Electro-Optic Materials

12. PERSONAL AUTHOR(S)

Larry E. Halliburton

13a. TYPE OF REPORT	13b. TIME COVERED	14. DATE OF REPORT (Year, Month, Day)	15. PAGE COUNT
Final	FROM July 85 TO Mar. 89	January 1990	

16. SUPPLEMENTARY NOTATION

17. COSATI CODES			18. SUBJECT TERMS (Continue on reverse if necessary and identify by block number)
FIELD	GROUP	SUB-GROUP	point defects; electron paramagnetic resonance; optical absorption; luminescence; lithium niobate; lithium tantalate; bismuth germanium oxide

19. ABSTRACT (Continue on reverse if necessary and identify by block number)

See abstract on back side.

20. DISTRIBUTION/AVAILABILITY OF ABSTRACT: ☐ UNCLASSIFIED/UNLIMITED ☒ SAME AS RPT. ☐ DTIC USERS	21. ABSTRACT SECURITY CLASSIFICATION: Unclassified
22a. NAME OF RESPONSIBLE INDIVIDUAL: Craig	22b. TELEPHONE (Include Area Code): 202-767-4931; 22c. OFFICE SYMBOL: NE

DD FORM 1473, 84 MAR 83 APR edition may be used until exhausted. All other editions are obsolete.

SECURITY CLASSIFICATION OF THIS PAGE

Point defects in lithium niobate and related electro-optic materials have been characterized using electron paramagnetic resonance (EPR), optical absorption, thermally stimulated luminescence (TSL), and diffusion techniques. In $LiNbO_3$, EPR has been used to investigate a radiation-induced trapped-hole center. This new S = 1/2 defect is stable at 77 K but thermally decays near 150 K. Its EPR spectrum exhibits a complex hyperfine structure which is best explained as one "hole" interacting equally with three ^{93}Nb nuclei. We suggest that the hole is equally shared by a set of three equivalent oxygen ions adjacent to a cation vacancy.

The photo-induced redistribution of charge has been characterized in $Bi_{12}GeO_{20}$ and $Bi_{12}SiO_{20}$ crystals. Optical excitation at 77 K converts Fe^{3+} ions to Fe^{2+} ions. The source of electrons (i.e., the hole traps) may be other impurities or intrinsic defects such as vacancies or anti-site cations. The Fe^{3+} recovery during warming correlates with thermoluminescence peaks at 145, 165, and 245 K. We postulate that Fe^{2+} ions are the recombination site and that each thermoluminescence peak corresponds to the release of holes from a different trap. Our results suggest that Fe^{3+} ions may play an important role in the photorefractive effect in these materials.

In $LiTaO_3$, the EPR spectrum of Ta^{4+} ions has been investigated. These defects were produced either by irradiating as-grown crystals with x-rays or by optically bleaching crystals that had been previously reduced. In both cases, the Ta^{4+} ions were stable only at temperatures near or below 77 K. The g and hyperfine matrix parameters describe a $5d^1$ electron on the tantalum ion, and we conclude that the defect represents a "self-trapped" electron at the normal Ta^{5+} site.

The diffusion coefficients of deuterium in single crystals of $LiTaO_3$ have been measured by monitoring the growth of OD^- infrared absorption bands. At 950 K, the diffusion coefficient is 1.7×10^{-8} cm^2/s for diffusion along the crystallographic c axis, and the activation energy is 1.5 eV. Electric-field-enhanced diffusion of deuterium was also demonstrated.

TABLE OF CONTENTS

page

I. INTRODUCTION AND SUMMARY

A three-year research program has been conducted with the goal of characterizing point defects in $LiNbO_3$ and related electro-optic materials. Specifically, we have conducted fundamental characterization studies that have led to well established models of point defects in these materials.

In $LiNbO_3$, electron paramagnetic resonance (EPR) has been used to investigate a trapped-hole center produced by ionizing radiation. This new S = 1/2 defect is stable at 77 K but thermally decays near 150 K. Its EPR spectrum exhibits a complex hyperfine structure which is best observed in the second-derivative mode. When the magnetic field is parallel to the c axis, the spectrum contains at least 26 equally spaced lines with 1.54 mT separation. This hyperfine pattern is best explained as one "hole" interacting equally with three ^{93}Nb nuclei (I = 9/2 and 100% abundant). We suggest that the hole is equally shared by a set of three equivalent oxygen ions adjacent to a cation vacancy.

In $Bi_{12}GeO_{20}$ and $Bi_{12}SiO_{20}$ crystals, the photo-induced redistribution of charge has been characterized using electron paramagnetic resonance, thermally stimulated luminescence, and optical absorption techniques. Excitation with 350-nm light at 77 K converts Fe^{3+} ions to Fe^{2+} ions. The source of electrons (i.e., the hole traps) is not known, but they may be other impurities or intrinsic defects such as vacancies or anti-site

cations. As the crystals are warmed to room temperature, recovery of the Fe^{3+} ions correlates with thermoluminescence peaks at 145, 165, and 245 K. We postulate that Fe^{2+} ions are the recombination site and that each thermoluminescence peak corresponds to the release of holes from a different trap. Our results suggest that Fe^{3+} ions may play an important role in the photorefractive effect in these materials.

In $LiTaO_3$, the electron paramagnetic resonance spectrum of Ta^{4+} ions has been investigated. These defects were produced either by irradiating as-grown crystals with x-rays or by optically bleaching crystals that had been previously reduced. In both cases, the Ta^{4+} ions were stable only at temperatures near or below 77 K. The g and hyperfine matrix parameters for the Ta^{4+} spectrum are $g_{\parallel} = 1.503$, $g_{\perp} = 1.172$, $A_{\parallel} \approx 0$, and $A_{\perp} = 699$ MHz. These parameters describe a $5d^1$ electron on the tantalum ion, and we conclude that the defect represents a "self-trapped" electron at the normal Ta^{5+} site.

The diffusion coefficients of deuterium in single crystals of $LiTaO_3$ have been measured by monitoring the growth of OD^- infrared absorption bands in samples heated in flowing D_2O vapor. At 950 K, the diffusion coefficient is 1.7×10^{-8} cm^2/s for diffusion along the crystallographic c axis, and the activation energy is 1.5 eV. Electric-field-enhanced diffusion of deuterium was also demonstrated. Proton replacement and electron-nuclear double resonance (ENDOR) experiments have shown that the structure previously reported in the electron

paramagnetic resonance spectrum of a radiation-induced center in $LiTaO_3$ is not due to a hyperfine interaction with protons.

II. A NEW TRAPPED-HOLE CENTER IN IRRADIATED $LiNbO_3$

1. INTRODUCTION

Lithium niobate ($LiNbO_3$) is a ferroelectric material widely used for such diverse applications as optical waveguiding, photorefractive storage of volume phase holograms, electro-optic modulation, and second harmonic generation.[1,2] The optical and electrical properties of $LiNbO_3$ are strongly influenced by the presence of impurities and other point defects. For example, $LiNbO_3$ crystals become black (i.e., opaque throughout the visible) when either heated above room temperature in a reducing atmosphere or exposed to ionizing radiation while at low temperature.

A variety of point defects exist in $LiNbO_3$. Lithium vacancies and anti-site niobium ions are present in large concentrations (exceeding 10^{21} cm^{-3}) because of the significant deviation from stoichiometry of congruent crystals.[3] Niobium vacancies may also be a major component of the defect structure in $LiNbO_3$.[4] Other defects ocurring in smaller concentrations are oxygen vacancies,[5-9] OH^- ions,[10-13] transition-metal ions,[14-16] self-trapped electrons,[17,18] bi-polarons,[19] and trapped holes.[17,20] Some of these defects are present in the as-grown material while others are produced by high-energy

radiation. Because of the critical role they may play in the performance of $LiNbO_3$ devices, it is important to establish detailed models of these defects. Electron paramagnetic resonance (EPR) provides a direct method to determine the structure of magnetic point defects. Other less direct techniques such as optical absorption, luminescence, and electrical conductivity must be used for diamagnetic defects.

In this section, we describe the use of the EPR technique to characterize a new trapped-hole center produced in $LiNbO_3$ by ionizing radiation. The optimum conditions to monitor this defect are described, the c-axis hyperfine pattern is presented, and a model is suggested.

2. EXPERIMENTAL

The $LiNbO_3$ crystals used in this study were grown by the Czochralski method from congruent melts. These samples came from three sources: undoped crystals were obtained from Union Carbide, Washougal, WA; undoped crystals and crystals doped with 0.1% titanium were obtained from the Crystal Growth Laboratory at Oklahoma State University; and crystals doubly doped with 5% magnesium and 0.01% iron were obtained from Crystal Technology, Palo Alto, CA. A Van de Graaff accelerator operating at 1.7 MeV in the electron mode was used to produce the defects. Specifically, the crystals were exposed to the x-rays generated when the accelerator's electron beam collided with an external brass target. During each irradiation, the sample temperature was maintained at 77 K and the dose received

was approximately 10^4 Gy (i.e., 10^6 rad). The unfiltered output of a tungsten lamp was used for the optical bleaching experiments.

The EPR data were taken with a Bruker ER200D spectrometer operating at 9.27 GHz. Typical sample size was 2 x 3 x 9 mm^3. First-derivative spectra were taken in the usual sense with a 100 kHz modulation frequency. Second-derivative spectra were taken with a 50 kHz modulation frequency and a 100 kHz detection frequency. When determining g values, the magnetic field and the microwave frequency were measured with a Varian E-500 gaussmeter and a Hewlett Packard 5340A counter. A quartz finger Dewar was used for EPR measurements at 77 K and an Oxford Instruments helium flow system was used for temperatures below 77 K.

3. RESULTS

When irradiated at 77 K with x-rays or other ionizing radiation, $LiNbO_3$ crystals turn black. This phenomenon is quite pronounced and has been reported in several earlier publications.[17,20] A 77-K irradiation also introduces EPR spectra,[17,20] as shown in Fig. 1. Signals from two defects dominate this EPR trace. The intense, broad line at g_c = 2.0294 has been assigned to a trapped hole center.[17] We will refer to it as Hole Center I. The other spectrum, a set of 10 equally spaced lines at g_c = 1.90, has been assigned to self-trapped electrons in the form of Nb^{4+} ions.[17] The broad trapped hole spectrum shows no angular dependence, whereas the

Nb^{4+} spectrum is strongly anisotropic. Additional weak EPR signals due to Fe^{3+}, Mn^{2+}, and Ni^{3+} are observed after the 77-K irradiation. Both the Fe^{3+} and the Mn^{2+} spectra are present before irradiation.

Closer examination of the EPR data in Fig. 1 reveals the presence of numerous weak signals superimposed on the broad spectrum of Hole Center I. An expanded version of this portion of the spectrum is shown in Fig. 2(a). These additional EPR lines, which we will refer to as Hole Center II, are centered on $g_c = 2.0365$ and are best observed when the magnetic field is parallel to the c axis. At other orientations of magnetic field, the lines from Hole Center II overlap sufficiently so that no structure can be resolved. Hole Center II was found after a 77-K x-irradiation in all the $LiNbO_3$ crystals available to us. This includes undoped samples from two commercial sources and from the Crystal Growth Laboratory at Oklahoma State University. The trace impurity content (e.g., Fe^{3+}, Mn^{2+}, etc.) of these undoped samples varied by as much as an order of magnitude. Other $LiNbO_3$ samples showing this new multiple-line EPR spectrum of Hole Center II were doped with titanium in one case and co-doped with magnesium and iron in another case.

Operating the EPR spectrometer in the second-derivative mode discriminated against the broad underlying spectrum from Hole Center I and provided a much clearer picture of the new spectrum from Hole Center II. This improvement, illustrated in Fig. 2(b), occurs because of the factor-of-twenty difference in

line widths for Hole Center I and Hole Center II. Also, the EPR spectrum of Hole Center II sharpens slightly as the temperature is reduced below 77 K. For these reasons, the EPR spectrum of Hole Center II was normally monitored in the present investigation at 35 K in the second-derivative mode. At least 26 equally spaced lines, separated by 1.54 mT, are observed in the second-derivative spectrum of Hole Center II. Unfortunately, it is difficult to determine the exact number of lines in this new spectrum because of overlapping signals from impurities such as nickel and manganese. Nonetheless, the central lines are clearly more intense than those near either end. Very slight deviations from complete mirror-symmetry are due to interference from the Mn^{2+} and Ni^{3+} ions. It is also because of this interference that the numbering of lines in Fig. 2(b) starts on the high field side of the spectrum.

Exposing an irradiated $LiNbO_3$ crystal to the unfiltered output of a tungsten lamp, while maintaining a sample temperature of 77 K, leads to a monotonic decrease in the intensities of Hole Center I, Hole Center I^T, and Nb^{4+} ions. The optically induced decay of these ESR spectra correlates with the decrease in the radiation-induced optical absorption (i.e., the decoloration of the sample). Also, the Nb^{4+} ions and both hole centers exhibit nearly identical thermal decays as the sample is returned to room temperature following a 77-K irradiation. Because of their similar responses to optical bleaching and thermal annealing, it proved impossible to enhance the concentration of Hole Center II relative to the other defects.

4. DISCUSSION

The most characteristic feature of Hole Center II is the multi-line pattern in its EPR spectrum. Because of their large number, their close spacing, and their symmetrical intensity pattern, it is likely that these lines arise from hyperfine interactions. Possible candidates for the responsible nuclei include ^{93}Nb (I=9/2 and 100% abundant) and ^{7}Li (I=3/2 and 92.6% abundant).

Three equivalent ^{93}Nb nuclei provide the best fit to the EPR spectrum in Fig. 2(b). The crystal symmetry of $LiNbO_3$ is trigonal[21] and this leads naturally to hyperfine interactions with three equivalent nuclei (assuming the defect symmetry to be the same as the crystal symmetry). Twenty-eight lines with intensity ratios of 1:3:6:10:15:21:28:36:45:55:63:69:73:75:75:73:...:3:1 are expected for three equivalent 100% abundant I = 9/2 nuclei.[22] The dashed lines in the stick diagram of Fig. 3 show this expected theoretical distribution of intensities of hyperfine lines and the solid lines show the actual intensities obtained from the c-axis spectrum of Hole Center II. These experimental values are the arithmetical average of the peak-to-bottom intensities on each side of the second-derivative EPR lines in Fig. 2(b). The agreement between the experimental and theoretical intensities in Fig. 3 is reasonable. The only significant disagreement occurs at the 11th, 17th, and 20th lines of the

pattern and this is due to interference from Mn^{2+} lines. The 27th and 28th lines are obscured by a line from Ni^{3+}.

In the remainder of this section, a model is developed for Hole Center II which incorporates three equivalent niobium ions. Trapped holes in oxide crystals are expected to occupy an oxygen 2p orbital since the valence band normally consists of orbitals of this type. Furthermore, in oxide crystals, holes introduced by radiation usually do not become self-trapped in the otherwise perfect lattice but instead hop from oxygen to oxygen until they either undergo recombination at an electron trap or are stabilized within the lattice by a pre-existing defect such as an impurity ion or a vacancy. For example, holes are trapped in the form of O^- ions adjacent to Mg^{2+} vacancies in MgO.[23] Similar behavior is observed in a number of other oxides.[24]

Lithium niobate should prove to be no exception to the behavior observed in other oxides. Thus, radiation-induced holes in $LiNbO_3$ crystals are expected to migrate to a stabilizing entity instead of becoming self-trapped in the perfect lattice. The identity of the stabilizing entity for an oxygen hole center is always difficult to establish. In the case of $LiNbO_3$, a cation vacancy is a prime candidate because its "effective negative charge" makes it an attractor of holes. Both lithium[3] and niobium[4] vacancies are believed to exist in $LiNbO_3$.

Each cation vacancy in $LiNbO_3$ has six neighboring oxygens, as shown in Fig. 4. Three of these oxygens form an equilateral

triangle in the basal plane on one side of the vacancy and the other three form a different equilateral triangle in the basal plane on the other side of the vacancy.[21] Thus, the oxygen ions adjacent to a cation vacancy fall into two distinguishable categories. These oxygen sets are labeled O(1) and O(2) for the lithium vacancy, and they are labeled O(2) and O(3) for the niobium vaccancy. Also, each oxygen has two slightly inequivalent lithium neighbors and two slightly inequivalent niobium neighbors.

If a hole were to be stabilized on a single oxygen ion adjacent to a cation vacancy, then only the one niobium neighbor (in the case of a niobium vacancy) or only the two niobium neighbors (in the case of a lithium vacancy) would be expected to contribute to a resolved hyperfine pattern. This simple model of a hole trapped on one oxygen does not agree with the observed spectrum wherein interactions with three equivalent niobiums are present.

A better model for Hole Center II is to assume that the trapped hole is not localized on a single oxygen ion but instead is delocalized onto the three oxygen ions forming the equilateral triangle above or below the cation vacancy. In the case of either the O(2) or the O(3) sets of oxygens adjacent to a niobium vacancy, this "delocalized hole" model provides three equivalent nearest-neighbor niobiums to contribute to a resolved hyperfine pattern. This agrees with the experimental results for Hole Center II and thus lends strong support to a niobium vacancy being the stabilizing entity for the hole. In

the case of the O(1) set of oxygens adjacent to a lithium vacancy, the "delocalized hole" model provides six nearest-neighbor niobiums (two for each oxygen ion) to contribute to the resolved hyperfine pattern. A preferential overlap of the hole's wavefunction onto just one of the two niobiums neighboring each of the three participating O(1) oxygens would be required to obtain agreement with experiment. In the case of the O(2) set of oxygens adjacent to a lithium vacancy, the "delocalized hole" model provides four nearest-neighbor niobiums (one of which is common to all three oxygens) to contribute to the resolved hyperfine pattern. Again, a preferential overlap of the hole onto the three equivalent niobium neighbors (and not the fourth common niobium) would be required to obtain agreement with experiment.

Thus, we are proposing a model for Hole Center II in which a hole is equally shared by the three oxygen ions immediately above or below a cation vacancy. We cannot determine which of the two oxygen sets is involved or whether it is a lithium or a niobium vacancy. The wavefunction of the hole overlaps onto one niobium nucleus adjacent to each oxygen to give the three equivalent niobium hyperfine interactions which are observed experimentally.

A final question arises about the nature of Hole Center I. Since there is no resolved hyperfine structure associated with this defect, one can only speculate about its detailed nature. Earlier investigators suggested that it might be a hole trapped on a single oxygen ion adjacent to a lithium vacancy.[17,20]

Based on our present study, we believe it is possible that Hole Center I may have a delocalized nature (i.e., the hole is shared by three oxygens instead of one). If this latter situation is true, it is tempting to assign Hole Center I to a delocalized hole stabilized by a lithium vacancy and Hole Center II to a delocalized hole stabilized by a niobium vacancy. To confirm or reject these models will require ENDOR data.

REFERENCES

1. M. E. Lines and A. M. Glass, Principles and Applications of Ferroelectrics and Related Materials (Oxford University Press, Oxford, 1977).

2. Integrated Optical Circuits and Components, edited by L. D. Hutcheson (Marcel Dekker, New York, 1987).

3. A. Rauber, in Current Topics in Materials Science, edited by E. Kaldis (North-Holland, New York, 1978), Vol. 1, pp. 481-601.

4. S. C. Abrahams and P. Marsh, Acta. Cryst. B42, 61 (1986).

5. G. Bergmann, Solid State Commun. 6, 77 (1968).

6. P. J. Jorgensen and R. W. Bartlett, J. Phys. Chem. Solids 30, 2639 (1969).

7. K. L. Sweeney and L. E. Halliburton, Appl. Phys. Lett. 43A, 336 (1983).

8. L. Arizmendi, J. M. Cabrera, and F. Agullo-Lopez, J. Phys. C 17, 515 (1984).

9. G. G. DeLeo, J. L. Dobson, M. F. Masters, and L. H. Bonjack, Phys. Rev. B 37, 8394 (1988).

10. J. R. Herrington, B. Dischler, A. Rauber, and J. Schneider, Solid State Commun. 12, 351 (1973).

11. W. Bollmann and H. J. Stohr, Phys. Stat. Solidi (a) 39, 477 (1977).

12. L. Kovacs, V. Szalay, and R. Capelletti, Solid State Commun. 52, 1029 (1984).

13. J. de Rosendo Ma., L. Arizmendi, J. M. Cabrera, and F. Agullo-Lopez, Solid State Commun. 59, 499 (1986).

14. J. B. Herrington, B. Dischler, and J. Schneider, Solid State Commun. 10, 509 (1972).

15. S. Juppe and O. F. Schirmer, Phys. Lett. A 117, 150 (1986).

16. G. Korradi, K. Polgar, A. A. Bugai, I. M. Zaritskii, L. G. Rakitina, V. G. Grachev, and N. I. Deryugina, Sov. Phys. Solid State 28, 412 (1986).

17. O. F. Schirmer and D. von der Linde, Appl. Phys. Lett. 33, 35 (1978).

18. J. L. Ketchum, K. L. Sweeney, L. E. Halliburton, and A. F. Armington, Phys. Lett. 94A, 450 (1983).

19. O. F. Schirmer, S. Juppe, and J. Koppitz, Cryst. Latt. Def. and Amorph. Mat. 16, 353 (1987).

20. L. E. Halliburton, K. L. Sweeney, and C. Y. Chen, Nucl. Instrum. Meth. B1, 344 (1984).

21. R. S. Weis and T. K. Gaylord, Appl. Phys. A 37, 191 (1985).

22. J. E. Wertz and J. R. Bolton, Electron Spin Resonance (McGraw-Hill, New York, 1972).

23. L. E. Halliburton, D. L. Cowan, W. B. J. Blake, and J. E. Wertz, Phys. Rev. B 8, 1610 (1973).

24. B. Henderson and J. E. Wertz, Defects in the Alkaline Earth Oxides (Taylor and Francis, Ltd., London, 1977).

FIGURE CAPTIONS

Figure 1. EPR spectrum of an undoped $LiNbO_3$ crystal after exposure to x-rays at 77 K. The measurement temperature was 77 K and the magnetic field was parallel to the c axis.

Figure 2. (a) First-derivative and (b) second-derivative EPR spectra of Hole Center I and Hole Center II. The measurement temperature was 35 K and the magnetic field was parallel to the c axis.

Figure 3. The dashed lines represent the expected distribution of hyperfine intensities for three equivalent 100% abundant I = 9/2 nuclei. The solid lines are experimental results taken from Hole Center II in Fig. 2(b).

Figure 4. Schematic representations of the $LiNbO_3$ lattice to illustrate the environment of (a) a niobium vacancy and (b) a lithium vacancy.

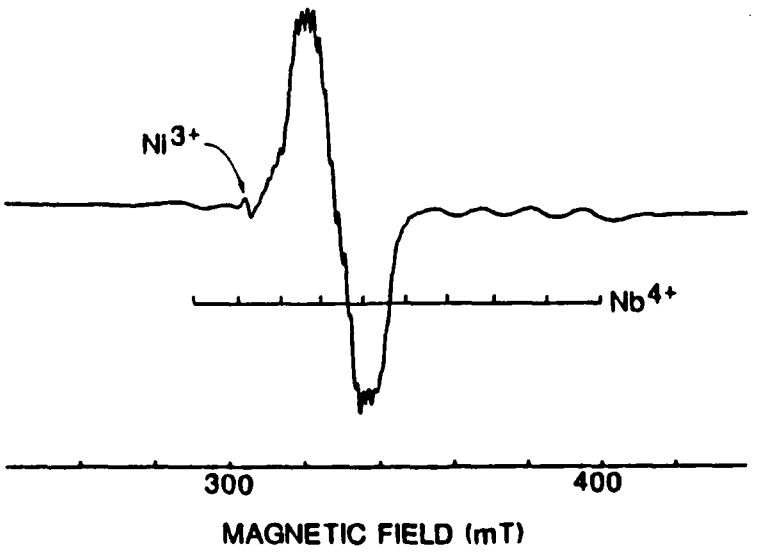

Figure 1

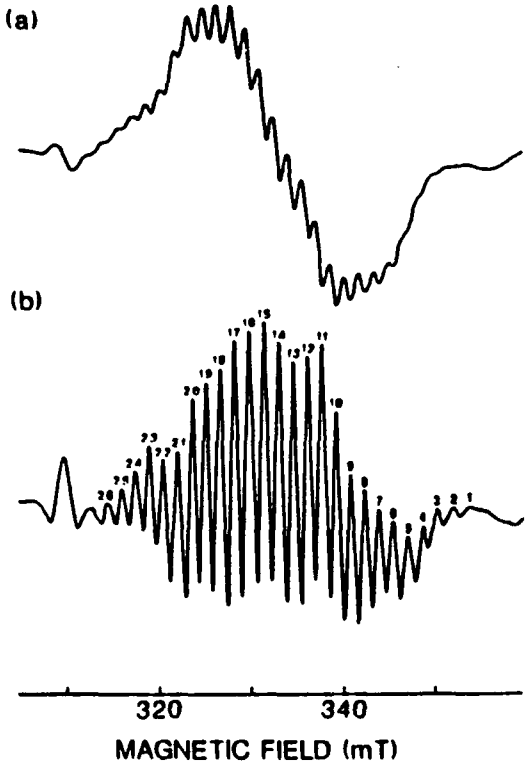

Figure 2

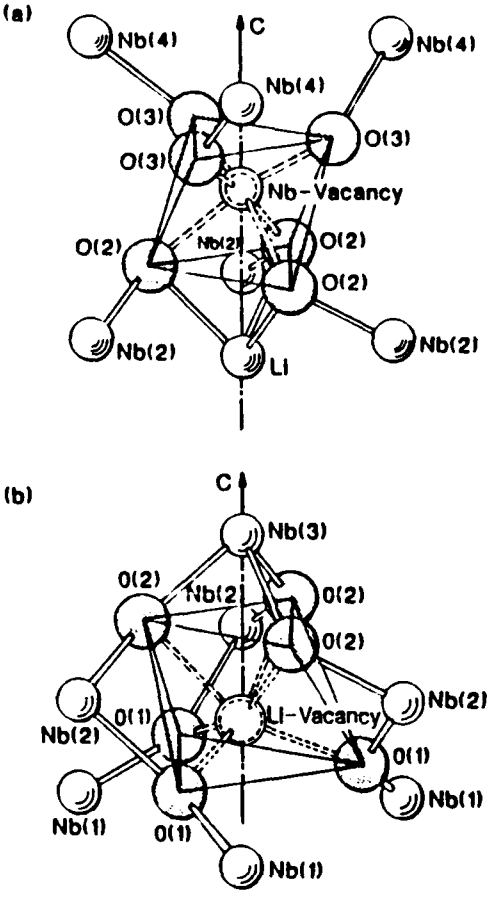

Figure 4

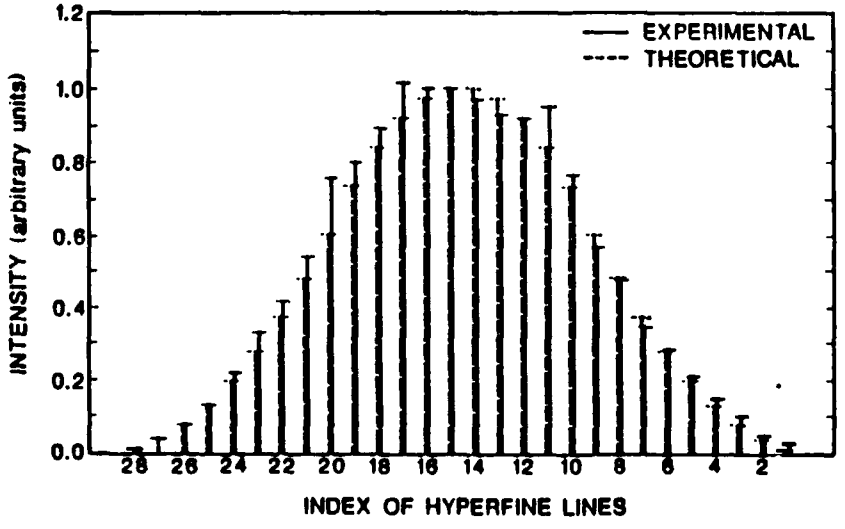

Figure 3

III. LIGHT-INDUCED MIGRATION OF CHARGE IN PHOTOREFRACTIVE $Bi_{12}SiO_{20}$ AND $Bi_{12}GeO_{20}$ CRYSTALS

1. INTRODUCTION

Photorefractive materials such as $LiNbO_3$, $BaTiO_3$, $Bi_{12}SiO_{20}$, and $Bi_{12}GeO_{20}$ are being extensively studied at the present time because of their potential applications in optical data processing.[1-4] When these crystals are exposed to interfering laser beams, electrons are released from impurity ions in the bright fringe regions. These electrons then move to the adjacent dark fringe regions where they become retrapped. The redistribution of charge resulting from these photoexcitation and retrapping processes creates an added component to the crystal's internal electric field which, in turn, changes the refractive index of the material via the electro-optic effect. The spatial variation of this added internal electric field corresponds to the interference pattern produced by the initial laser beams.

Early models of the photorefractive effect were based on the assumption that only one type of charge carrier (either holes or electrons) was participating in the charge migration process.[5-6] However, investigators[7-9] have had to consider the transport of both types of carriers in order to explain their results in materials such as $LiNbO_3$ and $BaTiO_3$. In contrast, photoconductivity results[10,11] from $Bi_{12}SiO_{20}$ and $Bi_{12}GeO_{20}$ indicate that the contribution from electrons is at least an

order of magnitude greater than that from holes. This led to the generally accepted notion that only electrons needed to be considered when explaining the photorefractive effect in these latter materials. More recently, Strohkendl and Hellwarth[12] have provided evidence that the one-charge-carrier model is not entirely applicable even in the case of $Bi_{12}SiO_{20}$.

Identifying the specific impurities and other defects which participate in the photorefractive effect is an important goal since this information will allow a material to be optimized for a particular set of applications. In this section, we describe the use of spectroscopic techniques such as electron paramagnetic resonance (EPR), thermally stimulated luminescence (TSL), and optical absorption to characterize point defects in commercially grown, undoped crystals of $Bi_{12}GeO_{20}$ and $Bi_{12}SiO_{20}$ (hereafter referred to as BGO and BSO, respectively). Much of our attention has been focused on the behavior of Fe^{3+} impurity ions after photoexcitation at 77 K. Correlations are found in the EPR and TSL data.

2. EXPERIMENTAL PROCEDURE

The BGO crystals were purchased from Crystal Technology, Palo Alto, CA and the BSO crystals were provided by Union Carbide, Washougal, WA. Samples for the EPR experiments were cut from the larger crystals and had dimensions of 2 x 3 x 8 mm^3. Optical samples for the absorption and the TSL experiments had dimensions of 2 x 10 x 15 mm^3. The two broad faces of the optical samples were polished.

An IBM Instruments (Bruker) Model ER200D spectrometer was used to obtain the EPR data. It operated at X-band (9.3 GHz) with a modulation frequency of 100 kHz. The magnetic field and the microwave frequency were measured with a Varian E-500 gaussmeter and a Hewlett Packard 5340A counter, respectively. A small quartz-tipped finger Dewar extending into the microwave cavity allowed the EPR sample to be immersed directly in liquid nitrogen during the measurements.

Optical absorption spectra were taken with a Perkin-Elmer Model 330 dual-beam spectrophotometer. In these measurements, the sample was mounted on a copper cold-finger which extended below the liquid nitrogen reservoir of a home-built metal Dewar. This allowed the sample's temperature to be maintained at approximately 80 K. The same optical Dewar was used to collect the TSL data. In these experiments, the emitted light was detected with an RCA 7102 photomultiplier tube placed immediately adjacent to the Dewar window and in front of the broad face of the sample. This particular phototube was chosen because of its greater sensitivity in the near infrared spectral region. A Keithley 600B electrometer converted the output of the phototube into a signal suitable for recording. No attempt was made to use a monochromator or filters to selectively examine the emission in the various regions of the optical spectrum.

A 150-W mercury-xenon lamp and a 25-cm monochromator (SPEX Minimate) set at 350 nm with a 5-mm exit slit was used to

induce the charge redistributions in the EPR and optical experiments.

3. EXPERIMENTAL RESULTS

A. Electron paramagnetic resonance

Although our BGO and BSO samples were not deliberately doped with transition-metal ions, we expected that trace amounts of these impurities (at the level of a few ppm) might appear in our initial EPR spectra. Somewhat to our surprise, we discovered that a single, rather intense EPR spectrum representing a concentration of approximately 5×10^{19} impurity ions per cm^3 was present in the as-grown BGO samples. This spectrum is shown in Fig. 1(a). A nearly identical EPR spectrum at a similar concentration was found in the as-grown BSO samples. Wardzynski et al.[13] have assigned this spectrum in BGO to Fe^{3+} ions substituting for Ge^{4+} ions and von Bardeleben[14] has assigned the equivalent spectrum in BSO to Fe^{3+} ions substituting for Si^{4+} ions. Both investigators concluded that the necessary charge compensation was nonlocal. The Fe^{3+} EPR spectrum shown in Fig. 1(a) was taken at 77 K with the magnetic field parallel to the [100] direction. It appears to be three equally spaced lines; however, the five lines required for an S = 5/2 ($3d^5$) spin system are present in Fig. 1(a) since each of the two outer lines represents two unresolved transitions. This set of five lines collapses into one line when the magnetic field is rotated approximately 30° from the [100] direction in the (001) plane.

When the BGO sample is exposed to 350-nm light at 77 K for 5 min, a significant reduction in the Fe^{3+} EPR spectrum occurs. This effect is illustrated in Fig. 1(b). Since another EPR spectrum does not appear, we are unable to specify the new charge state of the Fe ions. Both Fe^{2+} and Fe^{4+} states are possible, but we favor Fe^{2+} because of the accompanying optical absorption spectrum (see Section 3.C) and also because Mn^{2+} ions have been reported[15] to occupy the tetrahedral sites in BGO and BSO.

As long as the sample is maintained at 77 K, the new charge state of the Fe ions is stable; however, returning the sample to room temperature restores the Fe^{3+} EPR spectrum to its original size. To further characterize this recovery process, a pulsed thermal anneal experiment was performed. First, the sample was exposed to 350-nm light for 5 min at 77 K and the intensity of the residual Fe^{3+} signal was measured. Next, the sample was subjected to a series of four-minute anneals at progressively higher temperatures between 77 and 300 K. After each anneal, the sample was returned to 77 K where the intensity of the Fe^{3+} EPR signal was monitored. The dashed curve in Fig. 2 illustrates the thermal recovery of the Fe^{3+} spectrum in BGO after its near elimination by the UV light at low temperature. Half of the Fe^{3+} ions have returned by 165 K and nearly all of them have returned by 200 K.

Photo-excitation of the BSO samples with 350-nm light at 77 K also destroyed more than 95% of the original Fe^{3+} EPR spectrum. The recovery of this signal during a subsequent

thermal anneal is illustrated by the dashed curve in Fig. 3. In contrast to the results from BGO, the Fe^{3+} EPR spectrum recovers in two steps, one between 125 and 200 K and the other near 245 K.

B. Thermally stimulated luminescence

Earlier investigators[16,17] have reported a series of TSL peaks below room temperature in both BGO and BSO. Excitation with ultraviolet light at low temperature gave rise to prominent TSL peaks near 160 and 240 K with the maximum in the emission spectrum occurring in the infrared at about 1.3 eV. With only TSL data, these scientists could not identify any of the responsible defects. As a result of having access to both EPR and TSL instrumentation in the present investigation, we have been able to establish that Fe^{3+} ions are participants in the TSL process in these two materials.

The solid curve in Fig. 2 shows the TSL data from our BGO sample. The crystal was first exposed to 350-nm light for five min at 80 K to redistribute the charge, then the temperature was increased at a linear rate while the emitted light was monitored. A small cartridge heater in the bottom of the empty liquid nitrogen reservoir of the optical Dewar provided the thermal energy. The heating rate was approximately 9 K/min from 80 K to 300 K. An intense peak near 165 K with a shoulder at 145 K is present along with another small peak at 240 K. These TSL results are in agreement with those previously reported by Lauer.[16] From a comparison of the EPR and TSL data

in Fig. 2, we conclude that the recovery of the Fe3+ EPR signal correlates with the 165-K TSL peak in BGO.

The TSL data from our BSO sample is represented by the solid curve in Fig. 3. The same three peaks, at 145, 165, and 245 K, which were found in BGO are also present in BSO. However, the intensities of the peaks at 145 K and 245 K are considerably greater in BSO than in BGO. We assume that the different intensities for the peaks in the two samples is simply a result of different concentrations of either trapping or recombination sites. As shown in Fig. 3, the Fe^{3+} EPR spectrum in BSO recovers in two steps after the 77-K optical bleach. The first recovery step between 125 K and 200 K correlates with the combined 145- and 165-K TSL peaks and the second Fe^{3+} recovery step closely parallels the 245-K TSL peak.

C. Optical absorption

In addition to the EPR and TSL studies, we also investigated the effect that an 80-K optical bleach would have on the optical absorption spectra of the BGO and BSO samples. The lower curve in Fig. 4 is the absorption spectrum, taken at 80 K, of an as-grown BGO sample. According to Hou et al.,[10] the band edge is near 3.4 eV at 80 K. Thus, the additional absorption extending out from the band edge in the 2.5 to 3.4 eV region must come from the unresolved "shoulder" initially reported by Hou et al.[10] and subsequently studied by numerous groups.[18-20] The origin of this absorption shoulder is still a subject of considerable controversy. Germanium or silicon

vacancy complexes have been suggested by some to be the responsible defects, while others have proposed bismuth substituting for germanium or silicon.

Illuminating the BGO sample for five min at 80 K with 350-nm light induced a broad absorption extending across the entire visible region of the spectrum, as shown by the upper curve in Fig. 4. The difference between the two absorption spectra (i.e., as-received and after the 80-K optical bleach) is plotted in the inset. It consists of an absorption band peaking at 2.6 eV (477 nm) along with a shoulder on the low-energy side. A similar absorption spectrum was induced in BSO with 350-nm light. In $LiNbO_3$, Fe^{2+} ions are responsible for a broad absorption band peaking near 500 nm and, by analogy, we suggest that the 2.6-eV band in BGO and BSO is due to Fe^{2+} ions. The obvious and immediate result of this photo-induced absorption spectrum is to make the BGO and BSO samples appear black to the human eye.

The thermal stability of the 2.6-eV absorption band was determined in the case of BGO. After being exposed to 350-nm light for 5 min at 80 K, the crystal was subjected to the same sequence of annealing steps as the earlier EPR samples. It was heated to a specified temperature, held there for 4 minutes, then recooled to 80 K where the optical absorption was measured. This procedure was then repeated at the next higher anneal temperature. Although the results are not shown, we found that the photo-induced absorption decays over the range

from 125 to 200 K. This correlates well with the recovery of the Fe^{3+} EPR spectrum and the TSL peaks in BGO.

4. CONCLUSIONS

Excitation of BGO and BSO crystals at low temperature with 350-nm light converts Fe^{3+} ions to Fe^{2+} ions. The source of these electrons is not known, but among the possibilities are undetected transition-metal-ion impurities, neutral oxygen vacancies, germanium or silicon vacancy complexes, and anti-site bismuth ions. Warming the samples to room temperature results in a series of TSL peaks when these photo-induced electron and hole pairs recombine. Since the infrared emission spectrum is the same for all of the TSL peaks,[16] we postulate that the recombination process is initiated by the release of holes from three distinct trapping sites. One of these traps thermally releases holes at 145 K, another at 165 K, and the last at 245 K. The participation of Fe^{2+} ions in the 245-K TSL peak precludes the possibility that the release of electrons from Fe^{2+} ions initiates the recombination process at 145 K and 165 K.

A final observation relates to the defects responsible for the photorefractive effect in BGO and BSO. From the present work and other reports,[14,15,21] it appears that all BGO and BSO crystals, even undoped, contain significant amounts of Fe^{3+} ions which can easily change valence state upon illumination. At room temperature, these changes would be transitory and could account for the observed lifetimes of laser-induced grat-

ings.[22,23] Thus, we suggest that Fe^{3+} impurity ions play a critical role in the photorefractive effect in BGO and BSO.

REFERENCES

1. A. M. Glass, Opt. Engineering 17, 471 (1978).

2. P. Gunther, Phys. Rep. 93, 199 (1982).

3. M. B. Klein and R. N. Schwartz, J. Opt. Soc. Am. B 3, 293 (1986).

4. F. Vachss and L. Hesselink, J. Opt. Soc. Am. B 4, 325 (1987).

5. N. V. Kukhtarev, Sov. Tech. Phys. Lett. 2, 438 (1976).

6. N. V. Kukhtarev, V. B. Markov, S. G. Odulov, M. S. Soskin, and V. L. Vinestkii, Ferroelectrics 22, 949 (1979).

7. R. Orlowski and E. Kratzig, Solid State Commun. 27, 1351 (1978).

8. M. B. Klein and G. C. Valley, J. Appl. Phys. 57, 4901 (1985).

9. S. Ducharme and J. Feinberg, J. Opt. Soc. Am. B 3, 283 (1986).

10. S. L. Hou, R. B. Lauer, and R. E. Aldrich, J. Appl. Phys. 44, 2652 (1973).

11. B. Kh. Kostyuk, A. Yu. Kudzin, and G. Kh. Sokolyanskii, Sov. Phys. Solid State 22, 1429 (1980).

12. F. P. Strohkendl and Hellwarth, J. Appl. Phys. 62, 2450 (1987).

13. W. Wardzynski, M. Baran, and H. Szymczak, Physica 111B, 47 (1981).

14. H. J. von Bardeleben, J. Phys. D: Appl. Phys. 16, 29 (1983).

15. W. Wardzynski, H. Szymczak, M. T. Borowiec, K. Pataj, T. Lukasiewicz, and J. Zmija, J. Phys. Chem. Solids 46, 1117 (1985).

16. R. B. Lauer, J. Appl. Phys. 42, 2147 (1971).

17. B. W. Holmes, J. E. Ludman, and C. L. Woods, in Basic Properties of Optical Materials: Summaries of Papers, 1985, Nat'l Bur. of Standards Special Publication 697, edited by A. Feldman, pp. 242-245; see also B. W. Holmes, E. Hammond, and S. Weathersby, Bull. Am. Phys. Soc. 31, 696 (1986).

18. O. A. Gudaev, V. A. Detinenko, and V. K. Malinovskii, Sov. Phys. Solid State 23, 109 (1981).

19. R. Oberschmid, Phys. Stat. Sol. (a) 89, 263 (1985).

20. B. C. Grabmaier and R. Oberschmid, Phys. Stat. Sol. (a) 96, 199 (1986).

21. W. Wardzynski, H. Szymczak, K. Pataj, T. Lukasiewicz, and J. Zmija, J. Phys. Chem. Solids 43, 767 (1982).

22. R. A. Mullen and R. W. Hellwarth, J. Appl. Phys. 58, 40 (1985).

23. L. Arizmendi and R. C. Powell, J. Appl. Phys. 62, 896 (1987).

FIGURE CAPTIONS

Fig. 1. The EPR spectrum of Fe^{3+} ions in BGO taken at 77 K with the magnetic field parallel to the [100] direction. Trace (a) was before and trace (b) was after a 5-min exposure to 350-nm light. The spectrometer gain was the same for both spectra.

Fig. 2. Thermal recovery of the Fe^{3+} EPR spectrum (dashed curve) and TSL peaks (solid curve) after low-temperature photo-excitation of BGO.

Fig. 3. Thermal recovery of the Fe^{3+} EPR spectrum (dashed curve) and TSL peaks (solid curve) after low-temperature photo-excitation of BSO.

Fig. 4. Effect of UV light on the optical absorption spectra of BGO. The lower trace was taken before and the upper trace after a 5-min exposure to 350-nm light at 80 K. The photo-induced absorption band (i.e., the difference between these two traces) is shown in the inset.

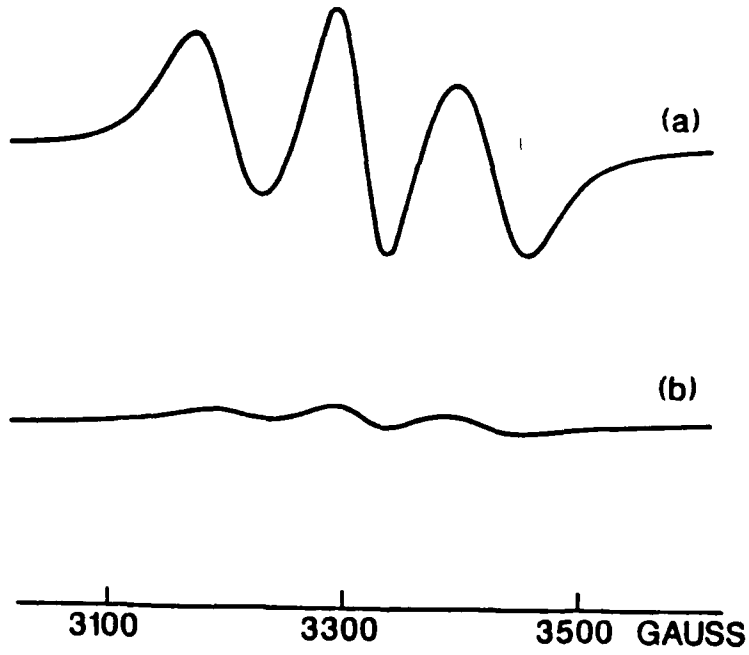

Figure 1

Figure 2

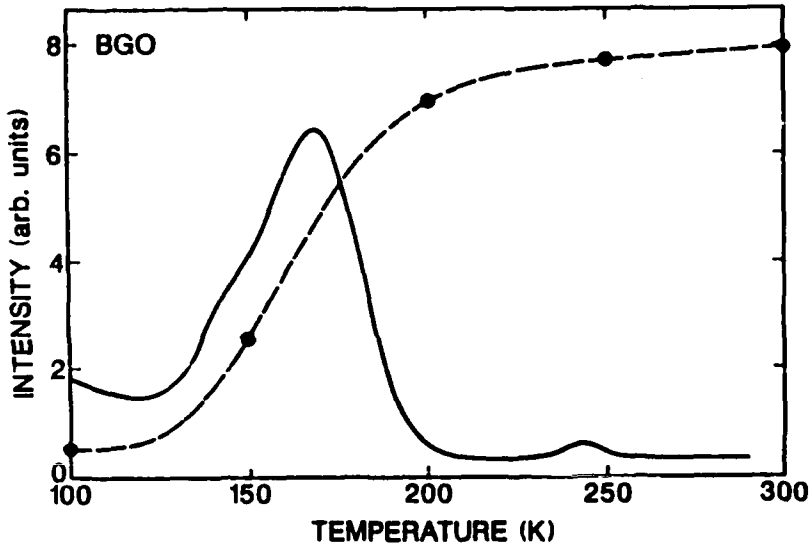

Figure 3

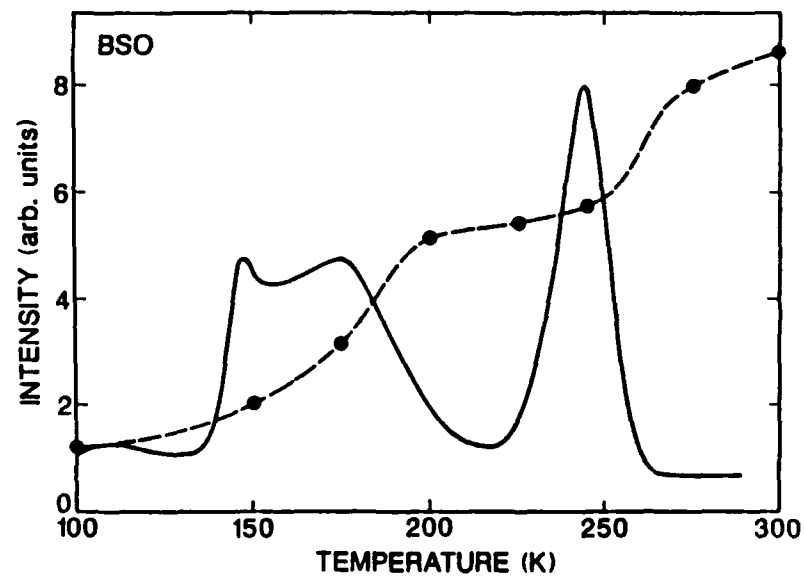

Figure 4

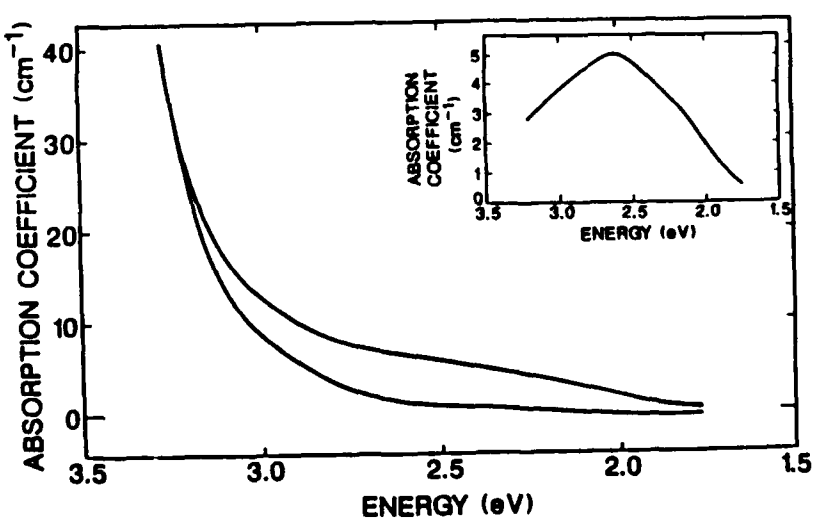

IV. SELF-TRAPPED ELECTRONS IN LITHIUM TANTALATE

1. INTRODUCTION

Lithium tantalate and lithium niobate have identical trigonal crystal structures and their lattice constants are nearly the same. Thus, the properties of specific point defects in these two electro-optic materials are expected to be very similar. A defect of particular interest is formed when an excess electron becomes trapped at either a niobium or a tantalum ion. Schirmer and von der Linde[1] initially observed such a defect, via electron paramagnetic resonance (EPR), when they exposed single crystals of $LiNbO_3$ to an intense ultraviolet laser beam or to x-rays. Based on the symmetry of their EPR spectrum and the magnitudes of the g and hyperfine matrix components, they suggested that this defect was a "self-trapped" electron and referred to it simply as a Nb^{4+} ion.

More recently, as part of a study of oxygen vacancies, Kappers et al.[2] reported the initial EPR observation of the analogous defect, i.e., a Ta^{4+} ion, in reduced $LiTaO_3$ crystals that had been optically bleached at low temperature. In this section of our report, we describe results obtained from a more complete EPR study of these Ta^{4+} ions. Two quite different production methods are demonstrated, spin-hamiltonian parameters are determined from the angular-dependence of the EPR spectrum and the large g shifts are discussed in terms of a $5d^1$ electron.

2. EXPERIMENTAL

Acoustic-grade lithium tantalate crystals, in the form of Z-plates 1 mm thick and 30 mm in diameter, were purchased from Crystal Technology, Palo Alto, California. The EPR samples cut from these plates were approximately 10 x 3 x 1 mm^3 with either X or Y being the long dimension. Magnetic resonance data were taken on a Bruker ER200D spectrometer operating at 9.46 GHz with a modulation frequency of 100 kHz. An Air Products Heli-Tran liquid helium transfer system controlled the sample temperature while the magnetic field and the microwave frequency were measured with a Varian E-500 gaussmeter and a Hewlett Packard 5340A counter, respectively. Because of the extremely large EPR linewidths encountered for the Ta^{4+} ions, no corrections were made in our data for the slight difference in magnetic field between the sample and proton-probe positions within the magnet gap.

3. EXPERIMENTAL RESULTS

We produced the Ta^{4+} centers in $LiTaO_3$ by two dissimilar methods. The first of these production schemes, initially employed by Sweeney and Halliburton[3] in $LiNbO_3$ and later by Kappers et al.[2] in $LiTaO_3$, consists of optically bleaching a reduced crystal at temperatures near or below 77 K. The $LiTaO_3$ crystals are easily reduced in an argon atmosphere at temperatures in the range 850 to 950^{o} C, and the unfiltered output of a 150 W xenon lamp is used for the bleaching at low tempera-

ture. In short, the reduction process makes oxygen vacancies, each of which trap two electrons, and the subsequent bleaching light transfers one of these electrons to a Ta ion site in the regular lattice. Our other method of producing the Ta^{4+} ions is to irradiate the as-grown $LiTaO_3$ crystals with ionizing radiation, either x-rays or high-energy electrons, at temperatures near or below 77 K. This latter method is similar to that used by Schirmer and von der Linde[1] in their production of Nb^{4+} ions in $LiNbO_3$. Finally, we note that the Ta^{4+} ions disappear upon warming the sample to room temperature no matter which production method is used.

Fig. 1 shows the EPR results obtained after optically bleaching a reduced $LiTaO_3$ crystal. The optical bleach was done at 17 K and the sample temperature was maintained at 17 K during the subsequent EPR measurements. Trace (a) was taken with the magnetic field parallel to the c axis of the crystal, while trace (b) was taken with the field perpendicular to this axis. Also, the gain of the EPR spectrometer was increased by a factor of six in trace (b). The Ta^{4+} spectrum collapses into a single prominent line with a small shoulder on the high-field side when the magnetic field is parallel to the c axis. However, when the field is perpendicular to the x axis, the Ta^{4+} spectrum spreads out into the eight lines characteristic of the ^{181}Ta nucleus (I = 7/2, 100% abundant). The total breadth of this "perpendicular" spectrum is nearly 3000 gauss. The two extraneous lines located on the low-field side of the

Ta^{4+} EPR spectra in fig. 1 are assumed to be due to transition-metal-ion impurities present in trace amounts.

Trapped hole and Ta^{4+} ions are both formed when an as-grown $LiTaO_3$ crystal is irradiated at low temperatures, either with x-rays or 1.7 MeV electrons. Fig. 2 shows the EPR spectra obtained from these defects after an x-ray irradiation at 77 K. Again, trace (a) was taken with the magnetic field parallel to the c axis of the crystal while trace (b) was taken with the field perpendicular to the c axis. The sample temperature was 17 K during these measurements and, in each trace, the gain of the EPR spectrometer was increased by a factor of ten at approximately 3800 gauss (indicated by the breaks in the two curves) in order to magnify the less intense Ta^{4+} signal located in the higher-field region of the spectrum. The EPR spectrum assigned to the trapped hole center in fig. 2 is the same as that reported earlier by Chen et al.[4] When our 77 K irradiated sample was initially examined at 77 K, only the trapped hole EPR spectrum was observed (in agreement with the report by Chen et al.); however, cooling the sample to near liquid-helium temperatures revealed the additional presence of the Ta^{4+} spectrum.

Comparing figs. 1 and 2, we conclude that the Ta^{4+} EPR spectrum produced by the x-rays, and shown in fig. 2, is identical to the spectrum induced by bleaching the reduced crystal at low temperature, as shown in fig. 1. A major difference in the two Ta^{4+} production methods is the nature of the corresponding "hole" center, in the case of irradiated samples it is

the O^- ion[4] whereas in reduced samples it is the F^+ center.[2] Also of interest, more Ta^{4+} ions are formed in the reduced samples than in the irradiated sample.

To complete our characterization of the Ta^{4+} ion, we investigated the angular dependence of its EPR spectrum. This was done at 17 K using the reduced sample described in fig. 1. Line-position data were obtained for rotations in the X plane of the crystal and also in the basal plane (i.e., the c plane). The results from the basal plane showed, within experimental error, that the Ta^{4+} spectrum is axially symmetric about the c axis. In the X plane, line positions were measured every 15° from approximately -90° to -45° and from near +45° to +90°. Angles closer to 0° (i.e., the c axis) were not included because the individual line positions were impossible to resolve as the spectrum collapsed. The results from the X-plane rotation were fitted to the following spin-hamiltonian, which includes electron Zeeman, hyperfine, and nuclear Zeeman terms:

$$\mathcal{H} = g_\perp \beta (H_x S_x + H_y S_y) + g_{//} \beta H_z S_z + A_\perp (I_x S_x + I_y S_y) + A_{//} I_z S_z - g_N \beta_N \vec{H} \cdot \vec{I}$$

The "best" set of g and hyperfine parameters for the Ta^{4+} ion is given in table 1, along with those of the Nb^{4+} ion in $LiNbO_3$ and the Ti^{3+} ion in Al_2O_3. Our Ta^{4+} values were obtained by using a least-squares-fitting computer program to repeatedly diagonalize the 16 x 16 hamiltonian matrix. The measured

microwave frequency and magnetic field values were provided as input data to this program. A summary of the X-plane angular-dependence data for the Ta^{4+} ion is given in fig. 3 where the individual symbols represent experimental data and the solid curves are calculated from the "best-fit" spin-hamiltonian parameters.

4. DISCUSSION

The measured g values for the Ta^{4+} ion can be generally understood in terms of the analysis presented by Abragam and Bleaney[6] for a d^1 ion in a cubic plus trigonal environment. The atomic D state is split into an upper Γ_3 doublet and an lower Γ_5 triplet by the cubic field; the Γ_5 state is further split into a doublet and singlet by the trigonal field. Considering only the Γ_5 triplet and including spin-orbit coupling, an axial field, and effects of bonding to the ligand ions, Abragam and Bleaney obtained expressions for $g_{\parallel}$ and $g_{\perp}$. These are

$$g_{\parallel} = (2 + k)\cos(2\delta) - k$$

and

$$g_{\perp} = |1 + \cos(2\delta) - \sqrt{2}k\sin(2\delta)|$$

where $\tan(2\delta) = \sqrt{2}\lambda/(\Delta + \lambda/2)$ and k is the reduction factor for the matrix elements of orbital momentum. The parameter Δ is the energy separation of the doublet and singlet emerging from the Γ_5 triplet upon application of the trigonal field.

Using the measured g values from table 1, we numerically solved the preceding pair of equations for k and δ. In the

case of Ta^{4+}, we found 0.81 and 0.096π for k and δ, respectively; whereas, for Nb^{4+}, we found 0.63 and 0.044π for k and δ. These results appear reasonable and we view them as verification of the basic validity of the Abragam and Bleaney analysis.[6] Taking[7] λ for Nb^{4+} to be 750 cm^{-1} gives 3358 cm^{-1} for Δ. Furthermore, by assuming Δ has the same value in $LiNbO_3$ and $LiTaO_3$, the value of λ for Ta^{4+} is estimated to be 2200 cm^{-1}. Identical crystal structures and nearly the same lattice constants suggest that Δ should be similar for the two materials.

In summary, we have characterized and EPR spectrum in $LiTaO_3$ and have attributed it to an unpaired electron ($5d^1$) localized on a single tantalum ion, with no additional perturbations in the surrounding lattice. Large negative g shifts, a resolved hyperfine interaction with only one tantalum nucleus, and axial symmetry about the c axis support this assignment of the spectrum to a model consisting of a self-trapped electron.

REFERENCES

1. O. F. Schirmer and D. von der Linde, Appl. Phys. Lett. 33, 35 (1978).

2. L. A. Kappers, K. L. Sweeney, L. E. Halliburton, and J. H. W. Liaw, Phys. Rev. B 31, 6792 (1985).

3. K. L. Sweeney and L. E. Halliburton, Appl. Phys. Lett 43, 336 (1983).

4. C. Y. Chen, K. L. Sweeney, and L. E. Halliburton, Phys. Stat. Sol. (a) 81, 253 (1984).

5. N. E. Kask, L. S. Kornienko, T. S. Mandel'shtam, and A. M. Prokhorov, Fiz. Tverd. Tela 5, 2306 (1964) [Sov. Phys. Solid State 5, 1677 (1964)].

6. A. Abragam and B. Bleaney, Electron Paramagnetic Resonance of Transition Ions (Clarendon, Oxford, 1970) pp. 417-426.

7. T. M. Dunn, Trans. Faraday Soc. 57, 1441 (1961).

Table 1
Spin-hamiltonian parameters for the Ta^{4+} ion ($5d^1$) in $LiTaO_3$, the Nb^{4+} ion ($4d^1$) in $LiNbO_3$, and the Ti^{3+} ($3d^1$) ion in Al_2O_3.

	$g_\parallel$	$g_\perp$	$A_\parallel$ (MHz)	$A_\perp$ (MHz)	Reference
Ta^{4+} (in $LiTaO_3$)	1.503	1.172	~ 0	699	this work
Nb^{4+} (in $LiNbO_3$)	1.90	1.72	330	690	[1]
Ti^{3+} (in Al_2O_3)	1.07	< 0.1			[5]

FIGURE CAPTIONS

Figure 1. Electron paramagnetic resonance spectra from Ta^{4+} ions in $LiTaO_3$. The magnetic field is parallel to the c axis in trace (a) and perpendicular in trace (b). These spectra were taken at 17 K after an optical bleach at 17 K. The crystal had previously been reduced in argon at 925°C for one hour.

Figure 2. EPR spectra of a hole center and the Ta^{4+} ion in $LiTaO_3$. These data were taken at 17 K after an x-ray irradiation at 77 K. The magnetic field is parallel to the c axis in trace (a) and perpendicular in trace (b). The gain of the spectrometer was increased by a factor of ten in the field region above approximately 3800 gauss (indicated by the breaks in the two curves).

Figure 3. Angular dependence of the Ta^{4+} EPR spectrum in $LiTaO_3$ for rotation in the X plane (the c axis is at 0°). The points represent experimental data, while the solid curves were calculated from the spin-Hamiltonian parameters given in table 1.

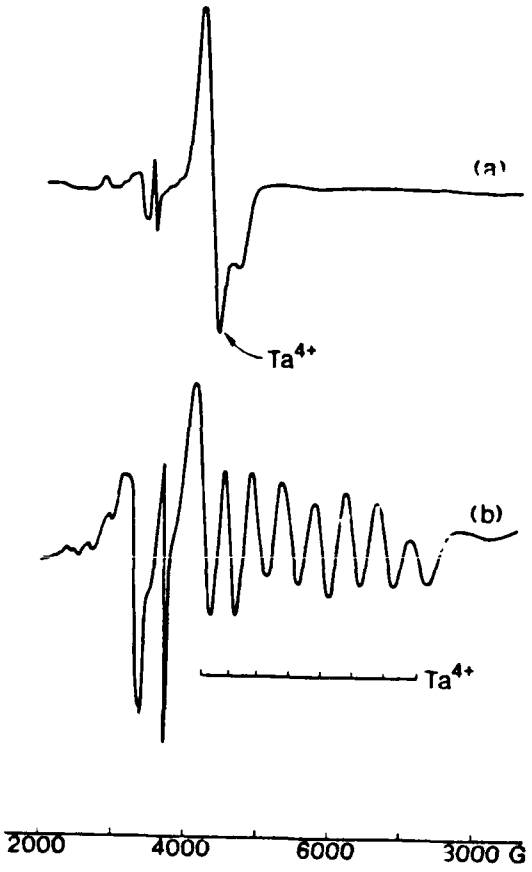

Figure 1

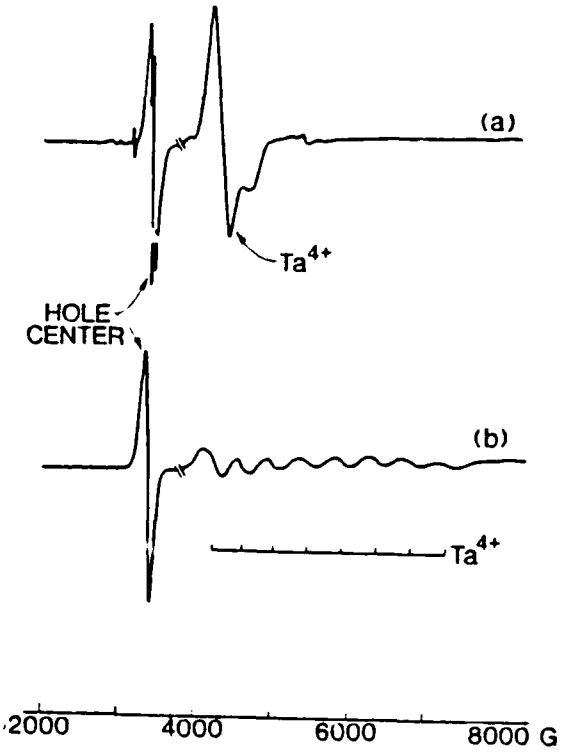

Figure 2

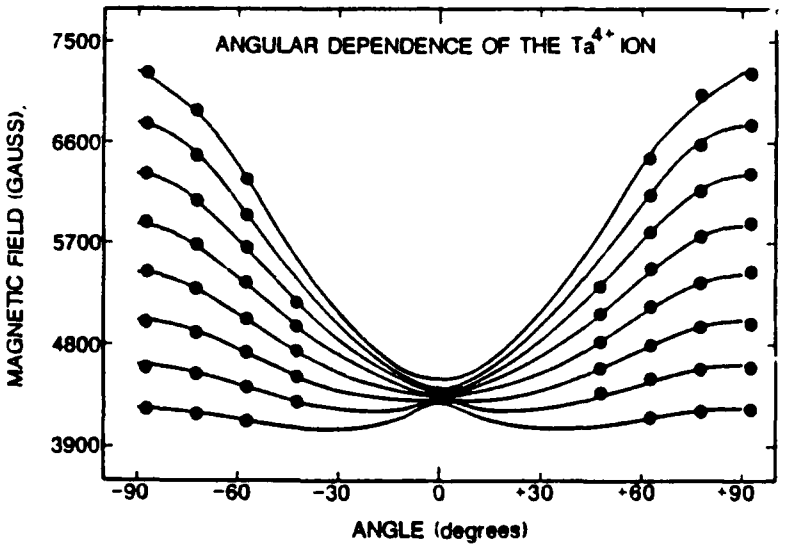

Figure 3

V. DEUTERIUM DIFFUSION AND MAGNETIC RESONANCE INVESTIGATIONS IN $LiTaO_3$ SINGLE CRYSTALS

1. INTRODUCTION

Single crystals of lithium niobate ($LiNbO_3$) and lithium tantalate ($LiTaO_3$) are being used in many electro-optic and acousto-optic devices.[1-3] An excellent combination of mechanical, electrical, and optical characteristics is primarily responsible for this situation.[4] The two materials possess identical trigonal crystal structures, and nearly all of their physical properties are similar. A notable exception is the significant difference in their Curie temperatures, 1197°C for $LiNbO_3$ and 620°C for $LiTaO_3$.

Hydrogen is an important impurity in these electro-optic materials. For example, early work by Smith et al.[5] suggested that the in-diffusion of hydrogen would increase the resistance of $LiNbO_3$ to optical damage (i.e., refractive-index changes caused by a high intensity laser beam). In related work, Jackel and coworkers[6] demonstrated that in-diffusion of hydrogen eliminated undesirable surface guiding in $LiNbO_3$ waveguides. Also, hydrogen has been implicated as a key impurity in the "thermal fixing" of holograms.[7] Despite the significant effort devoted to understanding the behavior of hydrogen in $LiNbO_3$ and $LiTaO_3$, a number of fundamental questions remain. Foremost among these are the identification of point defects that serve to stabilize a neighboring OH^-

molecule. Possibilities for these stabilizing defects include lithium vacancies or various impurities substituting for the niobium or tantalum ions.

Until now, nearly all the attention has been directed toward the behavior of hydrogen in $LiNbO_3$.[6-17] In this section, we focus on $LiTaO_3$ and describe the results obtained from the diffusion of deuterium at high temperature, with and without an external electric field. Also, we use the deuterated $LiTaO_3$ crystals to clarify the defect structure of a previously reported radiation-induced center.[18]

2. EXPERIMENTAL PROCEDURE

Commercial wafers of $LiTaO_3$ 1 mm thick and 25 mm in diameter were purchased from Crystal Technology, Palo Alto, CA. The c axis was perpendicular to the plane of these wafers. A diamond saw was used to cut optical samples with approximate dimensions of 10 x 7.5 x 1 mm^3 and infrared absorption data were taken at room temperature with a Perkin-Elmer 983 G spectrophotometer or a Beckman 4240 spectrophotometer. In each case, the infrared beam propagated along the c axis of the crystal and no polarizers were used.

Deuterium was diffused into the $LiTaO_3$ crystals, without the help of an external electric field, by exposing a polished sample to flowing D_2O vapor at high temperatures. The sample and surrounding vapor at one atmosphere were contained within a quartz tube which extended through a horizontal Lindberg furnace. In separate experiments involving external electric

fields, platinum electrodes were sputtered on the two broad faces of a crystal and then connected to a constant voltage power supply. The sample, thus prepared, was placed inside a stainless steel tube extending through a Lindberg furnace. Before heating, the tube was evacuated until the pressure was less than 5×10^{-6} Torr. Then D_2O water vapor was introduced into the closed sample tube until the pressure reached approximately 20 Torr. The pressure was finally allowed to approach 0.9 atmospheres by continuing to fill the tube with oxygen.

The electron-paramagnetic-resonance (EPR) data were taken at 77 K with a Bruker ER200D X-band spectrometer using samples approximately $8 \times 2 \times 1$ mm^3 in size. A Bruker ER 250 attachment for the EPR spectrometer provided the electron-nuclear double resonance (ENDOR) data, and a 2-MeV Van de Graaff operating in the electron mode was used to produce defects.

3. RESULTS AND DISCUSSION

A. Characterization of OH^- and OD^- bands

The lower half of Fig. 1 shows the infrared absorption spectrum of an as-grown $LiTaO_3$ crystal. A broad band peaking at about 3480 cm^{-1} with a pronounced shoulder at 3466 cm^{-1} was observed. The width of these combined bands was about 40 cm^{-1}. Previous investigators have assigned these to OH^- stretching vibrations.[5,8] After holding the sample at 900 K in flowing D_2O vapor for 2 hours, the relative intensities of the two overlapping OH^- bands were reversed. Also, a broad absorption band attributable to OD^- ions appeared at 2561 cm^{-1} with a

shoulder at 2570 cm^{-1}. These latter results are shown in the upper half of Fig. 1. The width of the combined OD^- bands was about 25 cm^{-1} and the frequency ratio of the OH^- to OD^- bands was 1.35. This ratio is near the theoretical expectation of $[\mu(OD)/\mu(OH)]^{1/2} = 1.37$ for the two isotopes. Here μ is the reduced mass of the molecular ion. The slight departure from 1.37 is indicative of the anharmonicity of the oscillators.

Figure 2 shows in more detail how the OH^- and OD^- infrared bands change as a $LiTaO_3$ crystal was heated in flowing D_2O vapor. The absorbances of the two bands, measured at 3466 and 2561 cm^{-1}, respectively, are plotted as a function of temperature. The sample was held for 10 min at each successively higher temperature with intervening infrared measurements at room temperature. The OD^- band did not emerge until the temperature reached 700 K. As expected, the OD^- concentration increased rapidly with temperature and its growth correlated with a decrease in the OH^- concentration. This suggests that an exchange of D^+ for H^+ was occurring. After the 1400 K step, the concentration of OD^- molecular ions was considerably greater than the initial OH^- concentration. Either all of the stabilizing sites in the lattice for hydrogen were not occupied in the original (i.e., as-grown) state of the crystal or the high-temperature treatment created new stabilization sites. Quite possibly, the deuterons (D^+) were replacing lithium ions (Li^+).

B. Diffusion measurements in D_2O vapor

The growth rate of the OD^- bands at a given high temperature provided the necessary information to determine the diffusion coefficient for deuterium at that temperature. The mathematical formalism has been provided by Crank[19] and the procedure for analyzing the diffusion data has been described by Gonzalez et al.[20] In brief, this method requires knowledge of the initial absorbance of the diffusing species, the absorbance after anneals of time t, and the absorbance at saturation (after long anneals). These are referred to as A_o, A_t, and A_∞, respectively. The diffusion coefficient D can be obtained from the formula

$$D = (\ell/2)^2[\pi M^2/(A_\infty - A_o)^2] \qquad (1)$$

where M is the initial slope for a plot of absorbance vs $\sqrt{t}$ and 2ℓ is the thickness of the sample.

In Fig. 3, the absorbance, monitored at 2561 cm^{-1}, is plotted against $\sqrt{t}$ for three $LiTaO_3$ crystals annealed at 850, 900, and 950 K, respectively. From the slopes of these lines, the diffusion coefficients were determined to be D(850 K) = 0.2 x 10^{-8} cm^2/s, D(900 K) = 0.6 x 10^{-8} cm^2/s, and D(950 K) = 1.7 x 10^{-8} cm^2/s. Similar values were obtained for the diffusion of deuterium in $LiNbO_3$.[10] The lines in Fig. 3 did not extrapolate back to the origin; the initial growth rate appeared to be more rapid and this suggests that more than one activation energy was involved. We also observed that the OD^- infrared peak

position and half-width remained unchanged during each anneal sequence. This latter result indicates that the trapping (i.e., stabilizing) site for the OD^- ions within the $LiTaO_3$ lattice does not change during the high-temperature diffusion treatments.

The activation energy E for the deuterium diffusion was obtained using the cross-cut method.[21] In Fig. 4, the times for the three crystals to reach the same arbitrary value of absorbance are plotted against the reciprocal of the annealing temperature. By fitting these data to an Arrhenius equation

$$D = D_o \exp(-E/kT), \qquad (2)$$

the activation energy E and the pre-exponential factor, D_o, were found to be 1.5 eV and 1.5 cm^2/s, respectively.

C. Electric-field-enhanced diffusion in D_2O vapor

The diffusion of deuterium in $LiTaO_3$ is enhanced at high temperature when an external electric field is applied. The two samples used in this portion of our investigation had identical initial infrared absorption spectra. Each sample was heated to 765 K and held for 43 h while surrounded by a static D_2O plus O_2 atmosphere. One of the crystals had an electric field of 12 V/cm applied parallel to the its c axis throughout the entire heating cycle. The second crystal had similar electrodes and was mounted in the same holder, but the electric potential was kept at zero during the heating cycle. These

procedures allowed the diffusion data obtained with and without the external electric field to be directly compared.

Figure 5(a) shows the infrared absorption spectrum of the as-grown crystals. There was a peak at 3480 cm^{-1} due to OH^- and nothing in the 2500 to 2600 cm^{-1} region. The results of the diffusion experiment with zero electric field are shown in Fig. 5(b). As expected, the OD^- peak at 2561 cm^{-1} appeared and the OH^- peak at 3480 cm^{-1} decreased. When the electric field was present, the OD^- peak at 2561 cm^{-1} became a factor of ten larger than in the zero-field case, as shown in Fig. 5(c). Also, the electric field caused the OH^- peak to increase relative to that found in the as-grown material. Presumably, residual hydrogen in the electrodes or in the surrounding atmosphere was swept into the crystal by the electric field.

These results were reproduced on several additional $LiTaO_3$ samples and a factor of ten enhancement in deuterium diffusion was always obtained for an applied electric field of 12 V/cm. More intense electric fields would be expected to produce even greater enhancements. Similar effects have been observed by Smith et al.[5] for the in-diffusion of hydrogen in $LiNbO_3$.

D. Magnetic resonance measurements

When $LiTaO_3$ crystals were exposed to ionizing radiation at low temperatures, a holelike paramagnetic defect was produced.[18] This defect correlates with a broad optical absorption band at 470 nm (2.64 eV). Its EPR spectrum (shown in Fig. 6) had a g value of 2.0224 and contained three equally

spaced lines with approximate intensity ratios of 1:2:1 when the magnetic field was parallel to the c axis. Unfortunately, these observations did not provide sufficient evidence to clearly establish an atomic model for the defect. From analogy with other oxide materials such as MgO and Al_2O_3, Chen et al.[18] suggested that a model for this defect might be a hole trapped at an oxygen ion adjacent to either a substitutional impurity or a structural defect such as a lithium vacancy.

The origin of the structure observed in the c-axis EPR spectrum of this holelike defect has been a subject of considerable debate. One possibility is to assume that the defect has S = 1/2 and that the three-line structure is due to hyperfine interactions with an adjacent pair of protons. It is generally known that two equivalent I = 1/2 nuclei would give three lines having a 1:2:1 intensity ratio.[22] However, the 52.5-gauss splitting is rather large for protons and would mean that the unpaired spin is localized to a large extent on the two protons which, in turn, would disagree with the "trapped-hole" model. Furthermore, a test of this proton hypothesis is difficult because EPR does not provide direct information about the identity of nuclear moments. A second possibility is to assume that this defect has S = 3/2 and that the observed structure is due to a crystal-field splitting of the energy levels. Finally, a third possibility would have the defect assigned to an impurity ion with two isotopes, one with I = 0 giving the central line and the other with I = 1/2 giving the outer pair of lines.

In an effort to determine whether or not protons are involved in this radiation-induced defect, we heavily deuterated a $LiTaO_3$ crystal. After a 77 K irradiation, the shape of the EPR spectrum was found to be identical to that produced before the deuteration. This lack of evidence for a deuterium version of the EPR spectrum occurred even though the infrared absorption spectrum showed that the concentration of OD^- in this particular crystal was about an order of magnitude greater than that of OH^-. A final search for direct evidence of hyperfine interactions with protons or deuterons was made using the electron-nuclear double resonance (ENDOR) technique. ENDOR experiments were performed on the radiation-induced center in both as-grown and deuterated crystals at temperatures near 4.2 K. No nuclear spin-flip signals arising from protons or deuterons were found. Thus, we conclude that is unlikely that this radiation-induced center involves protons.

4. SUMMARY

In general, the diffusion of deuterium in $LiTaO_3$ is similar to that in $LiNbO_3$. Isochronal annealing in flowing D_2O vapor indicates that below 1200 K the protons in $LiTaO_3$ are replaced by the entering deuterons. Above 1200 K, the concentration of deuterons significantly exceeds the initial concentration of protons, presumably because of an exchange of D^+ for Li^+. Isothermal annealing in the flowing D_2O vapor between 850 and 950 K indicates that at least two mechanisms of diffusion are involved. The second stage yields an activation energy of

1.5 eV and diffusion coefficients in the range of 10^{-8} to 10^{-9} cm^2/s. We also demonstrated that application of a weak electric field (12 V/cm) is very effective in enhancing the diffusion of deuterium at moderate temperatures.

In the second segment of our investigation, magnetic resonance techniques were used to show that the structure present in the EPR spectrum of a radiation-induced defect in $LiTaO_3$ is not caused by adjacent protons. No change in the shape of the EPR spectrum was found when the protons were replaced with deuterons. Also, ENDOR data showed no responses due to protons or deuterons.

REFERENCES

1. I. P. Kaminow, An Introduction to Electro-Optic Devices (Academic Press, New York, 1974).

2. M. E. Lines and A. M Glass, Principles and Applications of Ferroelectrics and Related Materials (Oxford University Press, Oxford, 1977).

3. E. Voges and A. Neyer, J. Lightwave Technol. Vol. LT-5, No. 5, 1229 (1987).

4. A. Rauber, in Current Topics in Materials Science, edited by E. Kaldis (North-Holland, New York, 1978), Vol. 1, pp. 481-601.

5. R. G. Smith, D. B. Fraser, R. T. Denton, and T. C. Rich, J. Appl. Phys. 39, 4600 (1968).

6. J. L. Jackel, D, H. Olson, and A. M. Glass, J. Appl. Phys. 52, 4855 (1981).

7. H. Vormann, G. Weber, S. Kapphan, and E. Kratzig, Solid State Commun. 40, 543 (1981).

8. J. R. Herrington, B. Dischler, A. Rauber, and J. Schneider, Solid State Commun. 12, 351 (1973).

9. W. Bollmann and H. J. Stohr, Phys. Stat. Solidi (a) 39, 477 (1977).

10. R. Gonzalez, Y. Chen, K. L. Tsang, and G. P. Summers, Appl. Phys. Lett. 41, 739 (1982).

11. D. A. Bryan, R. Gerson, and H. E. Tomaschke, Appl. Phys. Lett. 44, 847 (1984).

12. L. Kovacs, V. Szalay, and R. Capelletti, Solid State Commun. 52, 1029 (1984).

13. M. de Micheli, D. B. Ostrowsky, J. P. Barety, C. Canali, A. Carnera, G. Mazzi, and M. Papuchon, J. Lightwave Technol. Vol. LT-4, No. 7, 743 (1986).

14. Ma. J. de Rosendo, L. Arizmendi, J. M. Cabrera, and F. Agullo-Lopez, Solid State Commun. 59, 499 (1986).

15. L. Kovacs, I. Foldvari, and K. Polgar, Acta Phys. Hung. 61, 223 (1987).

16. F. Xiqi, Y. Jifeng, W. Yaoan, and L. Jiancheng, (to be published).

17. L. Kovacs, I. Foldvari, I. Cravero, K. Polgar, and R. Capelletti, (to be published).

18. C.Y. Chen, K. L. Sweeney, and L. E. Halliburton, Phys. Stat. Solidi 81, 253 (1984).

19. J. Crank, The Mathematics of Diffusion (Clarendon, Oxford, 1956).

20. R. Gonzalez, Y. Chen, and K. L. Tsang, Phys. Rev. B 26, 4637 (1982).

21. A. C. Damask and G. J. Dienes, Point Defects in Metals (Gordon and Breach, New York, 1963).

22. J. E. Wertz and J. R. Bolton, Electron Spin Resonance (McGraw-Hill, New York, 1972).

FIGURE CAPTIONS

Fig. 1. Infrared absorption spectrum of a $LiTaO_3$ crystal before (lower portion) and after (upper portion) exposure to flowing D_2O vapor for 2 h at 900 K.

Fig. 2. Peak absorbances of the OH^- and OD^- bands are plotted versus sample temperature. The crystal was held at each temperature for 10 min in flowing D_2O vapor.

Fig. 3. Absorbance of OD^- ions, measured at 2561 cm^{-1}, versus $\sqrt{t}$ for crystals annealed in flowing D_2O vapor at 850, 900, and 950 K.

Fig. 4. The time to reach a constant absorbance is plotted versus the reciprocal of the sample temperature for the three crystals. The data yield an activation energy of 1.5 eV.

Fig. 5. Infrared absorption spectra taken (a) before deuterium diffusion, (b) after deuterium diffusion with zero external electric field, and (c) after deuterium diffusion with a 12 V/cm external electric field. Trace c has been reduced by a factor of five.

Fig. 6. EPR spectrum of the radiation-induced defect in an as-grown $LiTaO_3$ crystal taken at 77 K with a microwave frequency of 9.30 GHz and with the magnetic field parallel to the c axis. The first derivative of the magnetic susceptibility (vertical axis) is plotted as a function of field.

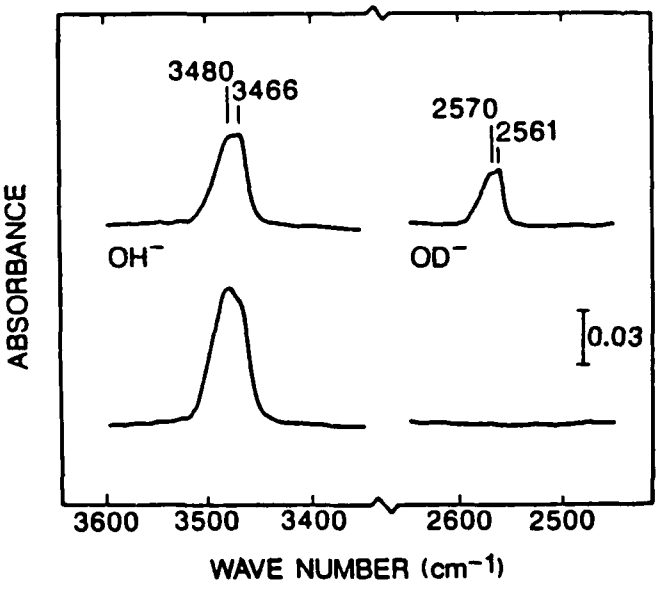

Figure 1

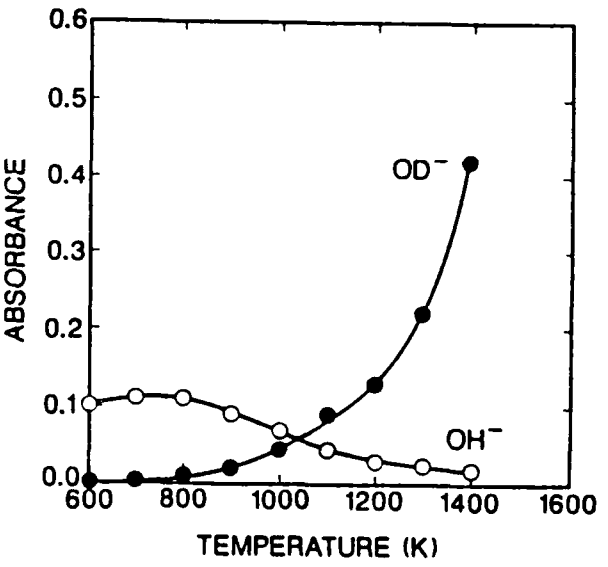

Figure 2

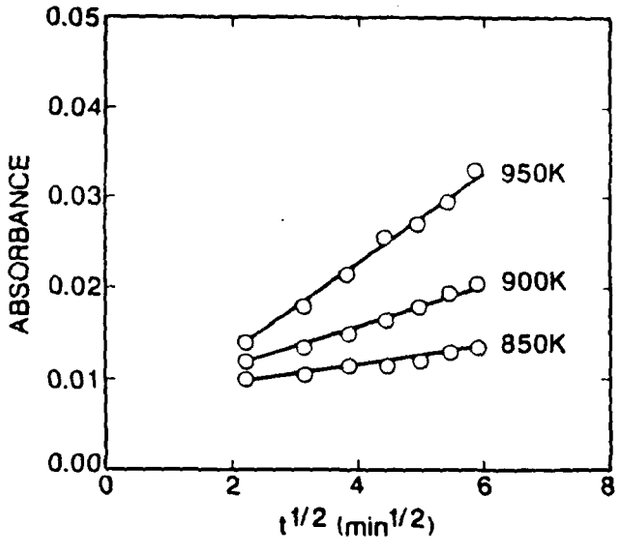

Figure 3

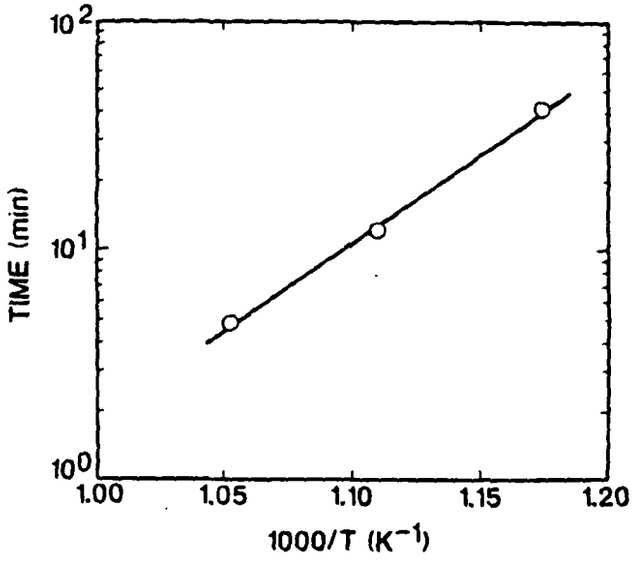

Figure 4

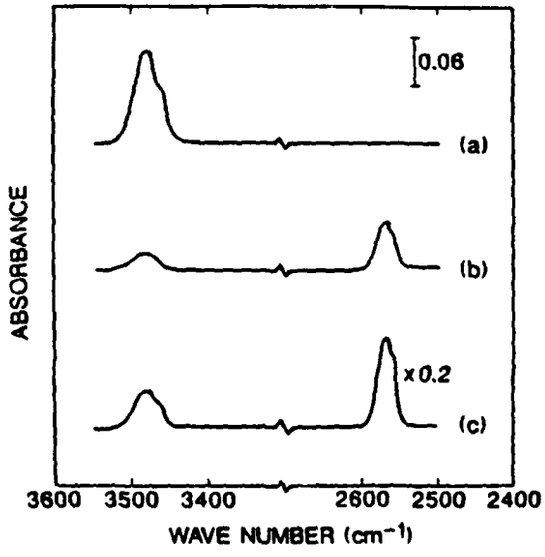

Figure 5

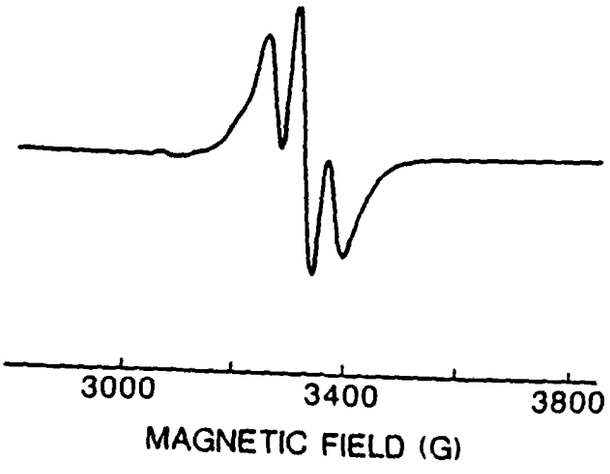

Figure 6

VI. LIST OF PAPERS AND THESES

A. Published Papers:

Self-Trapped Electrons in Lithium Tantalate, K. L. Sweeney, L. E. Halliburton, and L. A. Kappers, Physics Letters A 116, 81-84 (1986).

Light-Induced Migration of Charge in Photorefractive $Bi_{12}SiO_{20}$ and $Bi_{12}GeO_{20}$ Crystals, M. G. Jani and L. E. Halliburton, Journal of Applied Physics 64, 2022-2025 (1988).

Deuterium Diffusion and Magnetic Resonance Investigations in $LiTaO_3$ Single Crystals, R. Gonzalez, R. Hantehzadeh, C. Y. Chen, L. E. Halliburton, and Y. Chen, Physical Review B 39, 1302-1306 (1989).

A New Trapped-Hole Center in Irradiated $LiNbO_3$, T. Miki, M. R. Hantehzadeh, and L. E. Halliburton, Journal of Physics and Chemistry of Solids 50, 1003-1007 (1989).

B. Theses:

Investigation of Point Defects in Lithium Niobate by Electron Spin Resonance, Electron Nuclear Double Resonance, and Optical Absorption, M. R. Hantehzadeh, Ph.D. Dissertation, Oklahoma State University, 1987.